

Perfect absorption of water waves by linear or nonlinear critical coupling

Cite as: Appl. Phys. Lett. **114**, 013901 (2019); doi: [10.1063/1.5075541](https://doi.org/10.1063/1.5075541)

Submitted: 23 October 2018 · Accepted: 18 December 2018 · Published Online: 03 January 2019



View Online



Export Citation



CrossMark

E. Monsalve,^{1,a)}  A. Maurel,² P. Petitjeans,¹ and V. Pagneux³

AFFILIATIONS

¹ Laboratoire de Physique et Mécanique des Milieux Hétérogènes, CNRS, ESPCI-Paris, PSL Research University, Sorbonne University, Univ. Paris Diderot, 10 Rue Vauquelin, 75005 Paris, France

² Institut Langevin, CNRS, ESPCI-Paris, 1 Rue Jussieu, 75005 Paris, France

³ Laboratoire d'Acoustique de l'Université du Maine, CNRS, Avenue Olivier Messiaen, 72085 Le Mans CEDEX 9, France

^{a)} Electronic mail: eduardo.monsalve@espci.fr

ABSTRACT

We report on experiments of perfect absorption for surface gravity waves impinging a wall structured by a subwavelength resonator. By tuning the geometry of the resonator, a balance is achieved between the radiation damping and the intrinsic viscous damping, resulting in perfect absorption by critical coupling. Besides, it is shown that the resistance of the resonator, hence the intrinsic damping, can be controlled by the wave amplitude, which provides a way for perfect absorption tuned by nonlinear mechanisms. The perfect absorber that we propose, without moving parts or added material, is simple and robust and presents a deeply subwavelength ratio wavelength/thickness of $\simeq 18$.

Published under license by AIP Publishing. <https://doi.org/10.1063/1.5075541>

Waves are generically absorbed when they interact with a resonator close to the resonance frequency. To increase the absorption for scattering problems, a balance attained between radiation damping and intrinsic damping by critical coupling is a useful idea. Indeed, a resonator coupled to an infinite domain undergoes radiation damping^{1,2} even in the absence of intrinsic losses that would be present for a closed isolated resonator (e.g., viscous losses). When the balance is realized, perfect absorption is obtained: the incident wave does not generate any scattered wave. This concept has been already applied in the field of absorption in electromagnetism^{3–9} and in acoustics^{10–16} for instance.

In the context of water waves, devices able to absorb or to extract the energy from sea waves have been foreseen for a long time.² Primary wave-energy devices consisted in oscillating floating^{17,18} or submerged bodies,^{19,20} for a review, see Refs. 21 and 22. The need of the reduction of reflection of waves in harbours and basins has also attracted interest.^{23,24} More recently, modern devices have been sought considering the opportunity to combine them with existing breakwaters on the coast (see, e.g., Ref. 25). In most of the cases, the mechanism of energy absorption relies on resonances.

In this work, total absorption is obtained by choosing a simple resonator with a tunable geometry which allows us to cover a large range of radiation damping. In order to obtain critical coupling, the geometry of the resonator is tuned until the right balance between the radiation damping and the inherent viscous losses is achieved. Besides, we show that we can take advantage of the wave nonlinearities, which is the rule rather than the exception for sea waves, to tune the absorption toward the critical coupling.

The resonator that we consider is composed of a small open cavity of depth d at the extremity of a channel of width L (Fig. 1). A gate of width e delimits the open cavity connected to the channel through a thin guide corresponding to the resonator neck with an opening length s . The mechanism of the resonator is hybrid between a quarter-wavelength and a Helmholtz resonator. By varying the opening s , the radiation damping of the resonator will change a lot: for $s = L$, it is totally open to leakage, and for $s \rightarrow 0$, it will go to a closed resonator without leakage. Since the bathymetry is flat, with a finite depth H , the surface elevation η satisfies the Helmholtz equation

$$\Delta\eta + k^2\eta = 0, \quad (1)$$

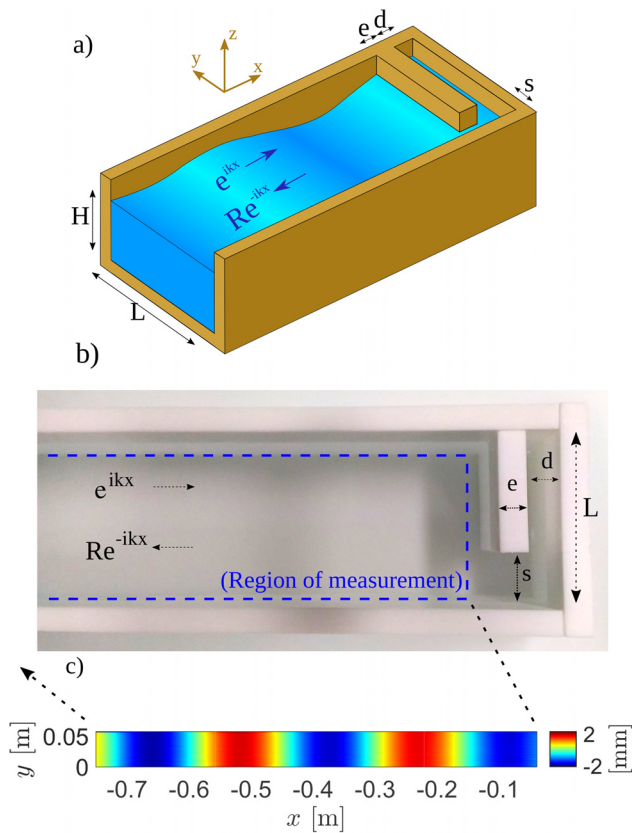


FIG. 1. Experimental setup of the subwavelength resonator absorber for water waves in a channel. (a) 3-dimensional scheme. (b) Top view of the end part of the channel with the resonator. (c) Typical surface elevation wave field measured experimentally in the channel with the FTP technique.

in which for a given frequency ω (harmonic regime $e^{-i\omega t}$), the wavenumber is given by the dispersion relation of water waves

$$\omega^2 = g k \tanh kH, \quad (2)$$

with g the gravity and H the water depth. In the following, we will be working in the low frequency regime, with $kL < \pi$, where only the planar mode can propagate in the channel. An incident wave impinges on the resonator which is at $x=0$ such that the total wave in the channel can be written in the form

$$\eta(x) = a(e^{ikx} + Re^{-ikx}), \quad x < 0, \quad (3)$$

with a the complex amplitude of the incident wave at $x=0$ and where R is the reflection coefficient.

We first consider the lossless case, and then, close to the resonance frequency, R can be expressed as

$$R = \frac{k - k_R - i\alpha_r}{k - k_R + i\alpha_r}, \quad (4)$$

where $k_R - i\alpha_r$ corresponds to the complex resonance frequency of the resonator²⁶ and k_R and α_r encapsulate the real resonance frequency and the radiative damping, respectively. This complex

resonance frequency has been computed numerically [solving Eq. (1) with the outgoing boundary condition with the pdeTool Finite Element Method toolbox of Matlab] as a function of the resonator opening s/L ; the results are shown in Fig. 2. We can observe that α_r spans a broad range of values, and it is thus confirmed that the chosen simple resonator offers a wide range of radiation damping. It is an important aspect because it means that it is a factor that we will be able to tune easily.

Then, a good approximation to take into account the intrinsic loss in the cavity can be obtained by simply shifting the numerator and the denominator by a positive viscous damping factor α_v (as if $k \rightarrow k + i\alpha_v$)

$$R = \frac{k - k_R - i(\alpha_r - \alpha_v)}{k - k_R + i(\alpha_r + \alpha_v)}. \quad (5)$$

We shall see that the above expressions (2) and (5) contain all the necessary terms to describe the critical coupling in our experiments. In every case, the point will be to try to obtain $\alpha_r = \alpha_v$ to get $R(k = k_R) = 0$, the total absorption at the resonance frequency.

The water depth is set to $H=5$ cm, and the channel is $L=6.2$ cm large and 1 m long. The dimensions of the resonator

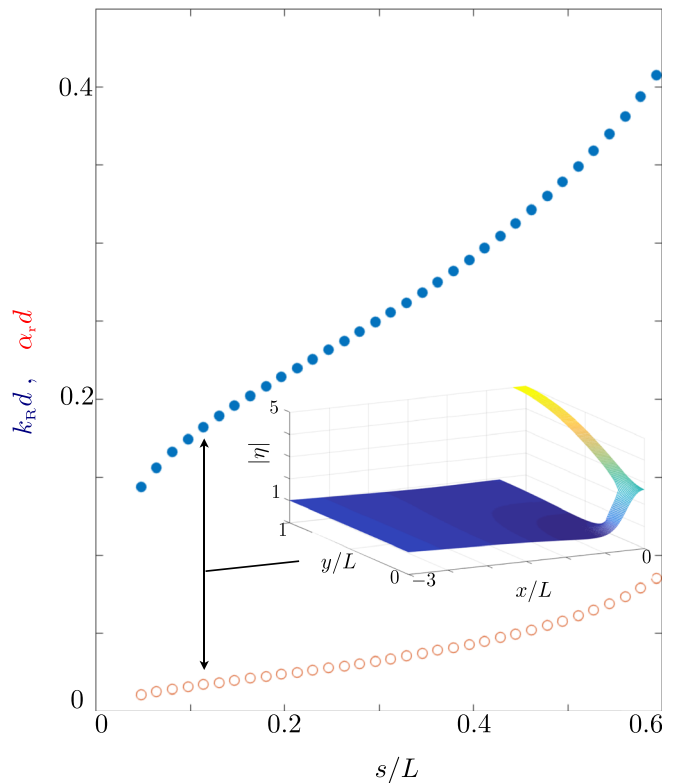


FIG. 2. Numerically computed complex resonances: dimensionless real part $k_R d$ (filled blue) and imaginary part $\alpha_r d$ (empty red) of the complex resonance frequency as a function of the opening of the resonator s/L . The inset shows the shape of the absolute value of the elevation $|\eta|$ at resonance frequency for $s/L = 0.11$.

are $d=e=1\text{cm}$, and variable opening s is from 0.3 to 3 cm. Waves are generated by a piston-type wavemaker driven by a linear motor in the range $f \in (1, 3.5)$ Hz with a step of 0.01 Hz, and their amplitudes a are controlled precisely from 0.2 mm to 5 mm with a step of 0.1 mm. In this frequency range, only the plane wave propagates [$k \in (10, 45) \text{ m}^{-1}$, whence $kL < \pi$]. The fields of surface elevation $\eta_T(x, y, t)$ are measured using the optical Fourier Transform Profilometry (FTP).^{27–29} Sinusoidal fringes are projected by a digital projector over an area of $72 \times 5.7 \text{ cm}^2$. The images of the free surface are collected by a camera, allowing for a spatial resolution given by the size of the projected pixel of 0.7 mm in both directions and a temporal resolution of 50 fps given by the acquisition frequency of the camera. The record duration of 16 s covers at least 20 periods for the lowest forcing frequency. From these space-time resolved measurements of the surface elevation η_T , we extract the linear mode from a temporal Fourier decomposition

$$\eta(x, y) = \frac{1}{t_f} \int_0^{t_f} \eta_T(x, y, t) e^{i\omega t} dt, \quad (6)$$

where ω is the forcing frequency and $t_f = 2n\pi/\omega$ with n the integer. This allows us to quantify the nonlinearity of the waves and to calculate the reflection coefficient R , far enough from the resonator (about 4 cm in practice) by using a fit of Eq. (3). Eventually, the signal-to-noise ratio is reduced by averaging $\eta(x, y)$ over the transverse direction y after the fit is performed to get (a, R, k) . Note that the typical measured field reported in Fig. 1 shows that η is indeed independent of y .

To begin with, we consider the linear regime for water waves and play with the opening s of the resonator to modify the critical coupling, trying to push α_r towards α_v in (5). In our experiments, the linear regime corresponds to wave amplitude $a \sim 0.5 \text{ mm}$, where we found the nonlinearities to be weak and where our measurement technique is accurate. Figure 3 reports the measured reflectivity $|R|^2$ for 4 values of s/L from 0.06 to 0.22. In each case, the reflectivity is smaller than unity because of the viscous losses, and it has a minimum at the resonance frequency, in rough agreement with (5). As can be seen, this resonance frequency is controlled by the neck opening s , resulting in the shift to higher frequencies when increasing s , in agreement with the numerical results in Fig. 2.

More interestingly, the minimum in the reflectivity $|R_{\min}|^2$ is impacted by the value of the opening s : this is what we use to achieve the critical coupling with zero reflectivity. To reach the total absorption, we perform a series of experiments varying s with a spacing of 1 mm and collect R_{\min} . The result is reported in Fig. 4. The critical coupling is obtained at the minimum for $s/L \simeq 0.11$ for $kd \simeq 0.17$, corresponding to a subwavelength ratio $\lambda/(d+e) \simeq 18$. The low reflection is further illustrated in the insets where we report the measured patterns of $|\eta(x, y)|$ for $|R_{\min}| \simeq 0.5$ at $s/L = 0.48$ and for $|R_{\min}| \simeq 2.10^{-2}$ at $s/L = 0.11$.

To interpret the findings of Fig. 4, it is sufficient to come back to (5). Adopting a representation of R in the complex map of k , a zero R appears at some distance of the real axis. In Fig. 5, the plot reports a typical case for the highest s/L value (high

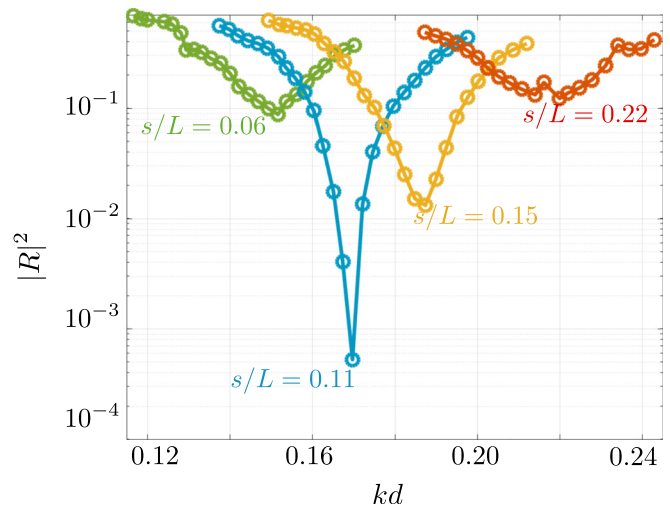


FIG. 3. Experimentally measured reflection $|R|^2$ against kd in the linear regime for different radiative damping dictated by the neck opening s/L of the resonator. The corresponding resonance frequencies $k_{r,d}$ computed numerically for the lossless case and displayed in Fig. 2 are $k_{r,d} = 0.15, 0.18, 0.20,$ and 0.22 for $s/L = 0.6, 0.11, 0.15,$ and 0.22 .

leakage); in this case, the radiative damping is higher than the viscous damping. Next, decreasing s/L makes the radiative damping decrease until it becomes balanced with the viscous damping (yellow point realizing the critical damping). Eventually, decreasing further the radiative damping moves the zero $|R|$ in the lower half plane.

It has been shown that water waves interacting with obstacles in the nonlinear regime experience an effective

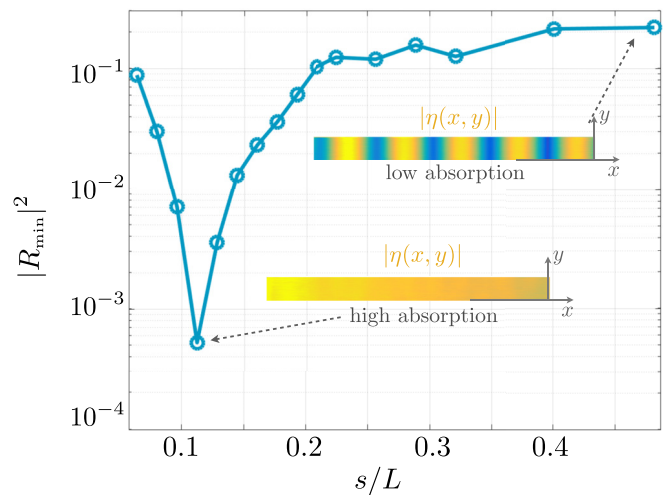


FIG. 4. Critical coupling in the linear regime—minimum reflection $|R_{\min}|^2$ against normalized opening s/L , with critical coupling realized at $s/L = 0.11$. The insets show the measured pattern of $|\eta(x, y)|$ in a case of low absorption (revealing interferences between the incident and reflected waves) and in a case of high absorption (with almost constant modulus demonstrating no reflection).

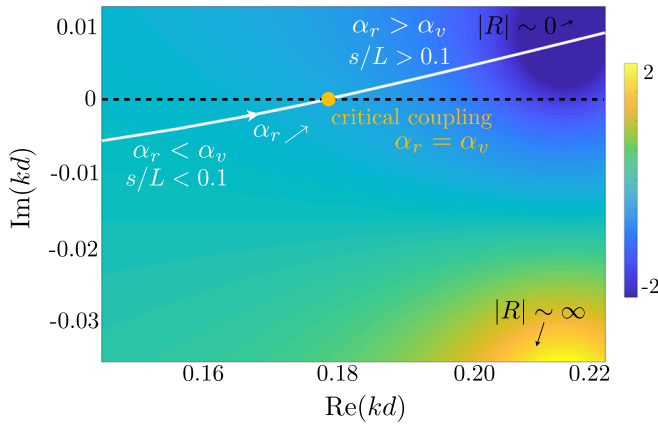


FIG. 5. Colormap of $|R|$ (log-scale) in the complex k -plane for $s/L = 0.2$. The white plain line shows the trajectory of the zero reflection varying s/L for a fixed viscous damping α_v (that of the linear regime) (see Ref. 30 for details). The critical coupling is achieved when the trajectory crosses the real axis (yellow point at $s/L \sim 0.1$). The black dashed line corresponds to the real frequencies of the experiments.

damping higher than that predicted in the linear regime (see, e.g., Ref. 31). This is attributable to the energy taken by structures generated in the fluid, and the stronger the nonlinearities, the higher the effective damping within³¹ a linear dependence.³² Hence, it is possible to increase the internal damping and to balance it with the radiative damping by increasing the amplitude of the waves. In other words, for the family of resonators which are strongly coupled to the exterior, it is possible to realize perfect absorption tuned by the nonlinearities. This critical coupling by nonlinear losses has been demonstrated recently for acoustic waves.³³

We consider resonators with relative openings $s/L = 0.06$, $s/L = 0.22$, and $s/L = 0.48$. We measure the reflectivity curves in the linear regime ($a = 0.5$ mm) and in the non-linear regime (with $a = 2$ mm for $s/L = 0.22$ and $a = 4$ mm for $s/L = 0.06$ and 0.48); the results are reported in Fig. 6. For $s/L = 0.06$, the reflectivity increases from the linear to the non-linear regime. This is expected since we already know from the study in the linear regime that for such a weakly coupled resonator, the

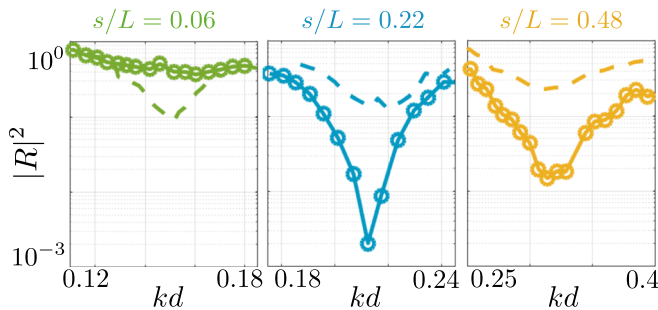


FIG. 6. Reflection coefficient $|R|^2$ as a function of the nondimensional wavenumber kd for different entrance widths s/L and incident wave amplitude. Dashed line: linear regime and circles: nonlinear regime.

radiative damping was already weaker than the viscous damping in the linear regime (see Fig. 5); hence, increasing the latter makes things worse. Reversely, for $s/L = 0.22$ and 0.48 , the reflectivity reduces, which is also shown in Fig. 5.

To go further, we modify with the constant step the wave amplitude in the nonlinear regime up to $a = 4.5$ mm (the wave-maker is controlled precisely with an amplitude step of 0.1 mm). We report $|R|^2$ as a function of the wave amplitude a in Fig. 7. This representation complements that of Fig. 6 at R_{\min} ($kd = 0.14, 0.21$, and 0.3 , respectively). Expectedly, for the resonator weakly coupled with the exterior ($s/L = 0.06$), the reflectivity increases with the nonlinearities since the system gets away from the critical coupling. Next, both resonators $s/L = 0.22$ and 0.48 are sufficiently coupled to the exterior, and hence, increasing the non-linearities makes these systems approach the critical coupling. However, the critical coupling is reached only for the resonator at $s/L = 0.22$. For $s/L = 0.48$, we see that we should increase further the nonlinearities to reach the critical coupling for that large opening. Eventually, the scenario described above is illustrated further in Fig. 8 where the trajectory of the zero $|R|$ in the complex k -plane is illustrated in 3 cases when the amplitude of the wave increases. In the case of critical coupling assisted by nonlinearity ($s/L = 0.22$), the zero $|R|$ is able to cross the real axis of frequency.

In this work, we have demonstrated experimentally that we can obtain perfect wave absorption by tuning the geometry of a resonator and consequently the radiation damping generated by this device. In addition, we demonstrated that the perfect absorption can be reached by tuning the incident wave amplitude (non-linearity), which varies proportionally the intrinsic damping of the system. In this situation, when there is an excess of radiation damping (wide entrance to the resonator), by increasing the incident wave amplitude, we obtain broadband absorption due to the smaller quality factor of the resonance in

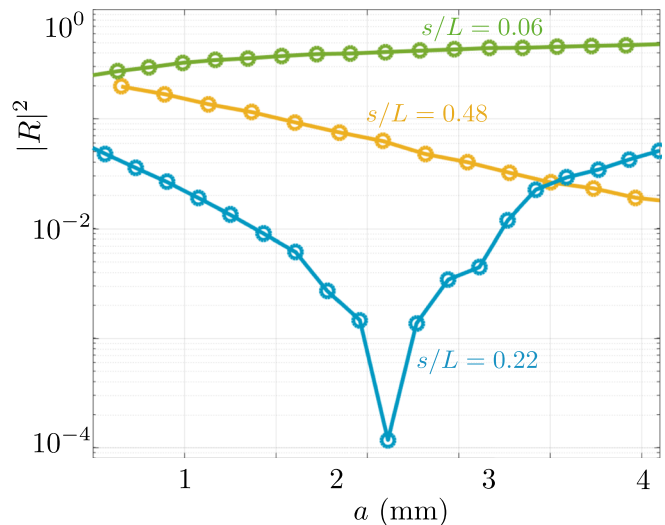


FIG. 7. Reflection coefficient as a function of the incident wave amplitude for different entrance widths s/L .

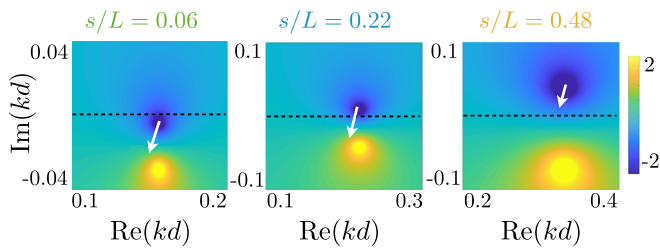


FIG. 8. Sketch of the typical trajectories of the zero reflectivity in the complex case when the loss is increased by nonlinearity, corresponding to our 3 experimental cases. The colormap is obtained with the expression of $|R|$ in the linear regime from Eq. (5) and as detailed in Ref. 30. The black dashed line corresponds to the real frequencies of the experiments.

this geometry. Note that, by using mirror symmetry, our design can be seen as a periodic array of resonators which may be used as an absorbing wall. A natural continuation of this work would be to apply it to an energy conversion system. In this case, in order to maximize the energy conversion, we have to minimize the intrinsic losses of the system (water viscous losses), keeping most of the mechanical resistance coming from the conversion device.

E.M. acknowledges the support of CONICYT Becas Chile Doctorado. E.M., P.P., A.M., and V.P. acknowledge the support of Agence Nationale de la Recherche through Grant No. DYNAMONDE ANR-12-BS09-0027-01.

REFERENCES

- ¹G. F. Carrier, R. P. Shaw, and M. Miyata, *J. Appl. Mech.* **38**, 335 (1971).
- ²C. C. Mei, M. Stiassnie, and D. K.-P. Yue, *Theory and Applications of Ocean Surface Waves* (World Scientific, 2005), Vol. 23.
- ³M. Cai, O. Painter, and K. J. Vahala, *Phys. Rev. Lett.* **85**, 74 (2000).
- ⁴A. Yariv, *IEEE Photonics Technol. Lett.* **14**, 483 (2002).
- ⁵N. I. Landy, S. Sajuyigbe, J. J. Mock, D. R. Smith, and W. J. Padilla, *Phys. Rev. Lett.* **100**, 207402 (2008).
- ⁶C. M. Watts, X. Liu, and W. J. Padilla, *Adv. Mater.* **24**(23), OP98 (2012).
- ⁷Y. D. Chong, L. Ge, H. Cao, and A. D. Stone, *Phys. Rev. Lett.* **105**, 053901 (2010).
- ⁸T. S. Luk, S. Campione, I. Kim, S. Feng, Y. C. Jun, S. Liu, J. B. Wright, I. Brener, P. B. Catrysse, S. Fan, and M. B. Sinclair, *Phys. Rev. B* **90**, 085411 (2014).
- ⁹J. R. Piper, V. Liu, and S. Fan, *Appl. Phys. Lett.* **104**, 251110 (2014).
- ¹⁰G. Ma, M. Yang, S. Xiao, Z. Yang, and P. Sheng, *Nat. Mater.* **13**, 873 (2014).
- ¹¹G. Ma and P. Sheng, *Sci. Adv.* **2**, e1501595 (2016).
- ¹²M. Yang and P. Sheng, *Annu. Rev. Mater. Res.* **47**, 83 (2017).
- ¹³H. Long, Y. Cheng, J. Tao, and X. Liu, *Appl. Phys. Lett.* **110**, 023502 (2017).
- ¹⁴T. Lee and H. Iizuka, *Appl. Phys. Lett.* **113**, 101903 (2018).
- ¹⁵V. Romero-Garcia, G. Theocharis, O. Richoux, A. Merkel, V. Tournat, and V. Pagneux, *Sci. Rep.* **6**, 19519 (2016).
- ¹⁶V. Romero-Garcia, G. Theocharis, O. Richoux, and V. Pagneux, *J. Acoust. Soc. Am.* **139**, 3395 (2016).
- ¹⁷D. V. Evans, *J. Fluid Mech.* **77**, 1 (1976).
- ¹⁸C. C. Mei, *J. Ship Res.* **20**, 63 (1976).
- ¹⁹M. J. Simon, *J. Fluid Mech.* **104**, 159 (1981).
- ²⁰S. Crowley, R. Porter, and D. Evans, *J. Fluid Mech.* **716**, 566 (2013).
- ²¹D. V. Evans and R. Porter, *Philos. Trans. R. Soc., A* **370**, 315 (2012).
- ²²J. Falnes, *Mar. Struct.* **20**, 185 (2007).
- ²³S. W. Twu and D. T. Lin, *Coastal Eng.* **15**, 389 (1991).
- ²⁴I. Theocharis, E. N. Anastasaki, C. I. Moutzouris, and T. Giantsi, *Ocean Eng.* **38**, 1967 (2011).
- ²⁵H. Martins-Rivas and C. C. Mei, *J. Fluid Mech.* **626**, 395 (2009).
- ²⁶V. Pagneux, *Dynamic Localization Phenomena in Elasticity, Acoustics and Electromagnetism* (CISM Springer, Vienna, Austria, 2013), Vol. 547, p. 181.
- ²⁷P. Cobelli, A. Maurel, V. Pagneux, and P. Petitjeans, *Exp. Fluids* **46**, 1037 (2009).
- ²⁸A. Maurel, P. Cobelli, V. Pagneux, and P. Petitjeans, *Appl. Opt.* **48**, 380 (2009).
- ²⁹A. Przadka, B. Cabane, V. Pagneux, A. Maurel, and P. Petitjeans, *Exp. Fluids* **52**, 519 (2012).
- ³⁰The trajectory has been obtained from Eq. (5) with running values of s/L and with (i) (k_R, α_r) taken from the numerical values of Fig. 2 and (ii) $\alpha_r d = \alpha_r r(s/L = 0.11) = 0.0165$ realizing the critical coupling as in Fig. 3.
- ³¹P. Warnitchai and T. Pinkaew, *Eng. Struct.* **20**, 593 (1998).
- ³²J. Morison, J. W. Johnson, and M. P. O'Brien, in *Proceedings of the Fourth Conference on Coastal Engineering*, ASCE, New York (1953), p. 340.
- ³³V. Achilleos, O. Richoux, and G. Theocharis, *J. Acoust. Soc. Am.* **140**, EL94 (2016).